Inorg. Chem. **2004**, *43*, 2284–2292

First Isolated Active Titanium Peroxo Complex: Characterization and Theoretical Study

Oxana A. Kholdeeva,*,† Tatiana A. Trubitsina,† Raisa I. Maksimovskaya,† Anatolii V. Golovin,† Wade A. Neiwert,‡ Boris A. Kolesov,§ Xavier López,|| and Josep M. Poblet*,||

Boreskov Institute of Catalysis, Pr. Lavrentieva 5, Novosibirsk 630090, Russia, Department of Chemistry, Emory University, 1515 Pierce Drive, Atlanta, Georgia 30322, Institute of Inorganic Chemistry, Pr. Lavrentieva 3, Novosibirsk 630090, Russia, and Departament de Química Física i Inorgànica, Universitat Rovira i Virgili, 43005 Tarragona, Spain

Received December 17, 2003

The protonated titanium peroxo complex $[Bu_4N]_4[HPTi(O_2)W_{11}O_{39}]$ (**1**) has been first prepared via interaction of the μ-oxo dimeric heteropolytungstate $[Bu_4N]_8[(PTiW_{11}O_{39})_2O]$ (**3**) with an excess of 30% aqueous H_2O_2 in MeCN. Peroxo complex **1** has been characterized by using elemental analysis, UV–vis, IR, resonance Raman (RR), ^{31}P and ^{183}W NMR spectroscopy, cyclic voltammetry, and potentiometric titration. The electronic and vibrational spectra of **1** are very similar to those of the well-known unprotonated titanium peroxo complex $[Bu_4N]_5[PTi(O_2)W_{11}O_{39}]$ (**2**), while ^{31}P and ^{183}W NMR spectra differ significantly. A compilation of the physicochemical techniques supports a monomeric Keggin type structure of **1** bearing one peroxo ligand attached to Ti(IV) in a η^2-coordination mode. The protonation of the titanium peroxo complex results in an increase of the redox potential of the peroxo group, $E_{1/2}$ = 1.25 and 0.88 V relative to Ag/AgCl reference electrode for **1** and **2**, respectively. In contrast to **2**, **1** readily reacts with 2,3,6-trimethylphenol (TMP) at 40 °C in MeCN to give 2,2′,3,3′,5,5′-hexamethyl-4,4′-biphenol (BP) and 2,3,5-trimethyl-*p*-benzoquinone (TMBQ). The proportion between BP and TMBQ in the reaction products depends on the TMP/**1** ratio. When a 2-fold excess of TMP is used, the main reaction product is BP (90%), while using a 2-fold excess of **1** leads to TMBQ (95%). On the basis of the product study, a homolytic oxidation mechanism that implicates the formation of phenoxyl radicals is suggested. The RR deuterium labeling experiments show that the activating proton is most likely localized at a Ti–O–W bridging oxygen rather than at the peroxo group. Theoretical calculations carried out at the DFT level on the protonated and unprotonated titanium peroxo derivatives also propose that the most stable complex is formed preferentially after protonation of the Ti–O–W site; however, both Ti–OH–W and TiOO–H protonated anions could coexist in solution.

Introduction

The selective catalytic oxidation of organic compounds with an environmentally attractive oxidant, aqueous H_2O_2, is of both academic and industrial interest.[1−6] The microporous titanium−silicate TS-1 developed by Enichem is a highly efficient catalyst for H_2O_2-based oxidations of relatively small molecules (<6 Å).[2−10] In recent years, mesoporous titanium−silicates have attracted much attention as catalysts for oxidation of bulky organic substrates.[11−16]

* Authors to whom correspondence should be addressed. E-mail: khold@catalysis.nsk.su (O.A.K.); poblet@correu.urv.es (J.M.P.). Fax: (+7)-3832-34-30-56 (O.A.K.); (+34)977-55-95-63 (J.M.P).

† Boreskov Institute of Catalysis.

‡ Emory University.

§ Institute of Inorganic Chemistry.

|| Universitat Rovira i Virgili.

(1) Sheldon, R. A.; Kochi, J. K. *Metal-Catalyzed Oxidations of Organic Compounds*; Academic Press: New York, 1981.
(2) Sheldon, R. A.; Dakka, J. *Catal. Today* **1994**, *19*, 215−246.
(3) Notari, B. *Adv. Catal.* **1996**, *41*, 253−334 and references therein.
(4) Centi, G.; Misono, M. *Catal. Today* **1998**, *41*, 287−296.
(5) Clerici, M. G. *Top. Catal.* **2000**, *13*, 373−386.
(6) Sanderson, W. R. *Pure Appl. Chem.* **2000**, *72*, 1289−1304.
(7) Bellussi, G.; Cazati, A.; Clerici, M. G.; Maddinelli, G.; Millini, R. *J. Catal.* **1992**, *133*, 220−230.
(8) Clerici, M. G.; Ingallina, P. *J. Catal.* **1993**, *140*, 71−83.
(9) Maspero, F.; Romano, U. *J. Catal.* **1994**, *146*, 476−482.
(10) Saxton, R. J. *Top. Catal.* **1999**, *9*, 43−57 and references therein.
(11) Tanev, P. T.; Chibwe, M.; Pinnavaia, T. *Nature* **1994**, *368*, 321−323.
(12) Corma, A. *Chem. Rev.* **1997**, *97*, 2373−2419.
(13) Sayari, A. *Chem. Mater.* **1996**, *8*, 1840−1852.
(14) Biz, S.; Ocelli, M. L. *Catal. Rev.−Sci. Eng.* **1998**, *40* (3), 329−407.
(15) Ying, J. Y.; Mehnert, C. P.; Wong, M. S. *Angew. Chem., Int. Ed.* **1999**, *38*, 56−77.
(16) Trong On, D.; Desplantier-Giscard, D.; Danumah, C.; Kaliaguine, S. *Appl. Catal., A: General* **2001**, *222*, 299−357.

10.1021/ic0354466 CCC: $27.50
Published on Web 03/10/2004

However, despite the number of experimental and theoretical studies of titanium−silicates, the nature of the oxidizing species and the oxidation mechanisms still remain under debate.[3,10,17−19] The search for soluble molecular models of heterogeneous titanium-containing catalysts is therefore an important goal. Recently, a few titanium−silsesquioxane complexes have been prepared and used as homogeneous probes of heterogeneous Ti,Si catalysts for studying alkene epoxidation with alkylhydroperoxides; however, a susceptibility to hydrolysis restricts their use to anhydrous media.[20−24] Meanwhile, anionic metal oxygen clusters (polyoxometalates or POMs for short) possess hydrolytic and thermodynamic stability and can be viewed as discrete fragments of a closed-packed array of metal oxide lattices.[25−33] Thus, methoxo derivatives of polyoxomolybdates have been used for modeling methanol oxidation on MoO_3[34] as well as for modeling of surface oxide reactivity in propene ammoxidation.[35] Transition metal monosubstituted POMs are of special interest because they may, in principle, serve as models of active catalytic centers isolated in an inorganic matrix. Recently, titanium monosubstituted Keggin-type POMs (Ti−POMs) were successfully used as tractable probes for studying the mechanism of thioether oxidation with H_2O_2.[36−38]

Thus far, all isolated and well-characterized titanium peroxo complexes, including the well-known Ti−POM peroxo complex $[Bu_4N]_5[PTi(O_2)W_{11}O_{39}]$[39,40] (**2**), were found to be inactive toward organic substrates under stoichiometric conditions.[36,41−45] The crucial role of protonation for the catalytic activity of titanium peroxo species was established in both heterogeneous and homogeneous catalytic oxidations with H_2O_2,[3,7,10,36,42,46] and hydroperoxo titanium species of various structures were proposed as the reactive intermediates.[3,7,9,17,42,47,48] However, no titanium hydroperoxo complex has yet been isolated. Recently, we found that a protonated Ti−POM species, generated in situ by adding 1 equiv of protons (in the form of triflic acid) to **2**, is capable of oxidizing thioethers under both catalytic and stoichiometric conditions.[36] Here we report the first synthesis and comprehensive characterization of the protonated Ti−POM peroxo complex $[Bu_4N]_4[HPTi(O_2)W_{11}O_{39}]$ (**1**) and demonstrate its reactivity toward a representative alkylphenol, 2,3,6-trimethylphenol (TMP). Previously, we studied TMP oxidation with aqueous H_2O_2 in the presence of mesoporous titanium−silicates.[49,50] The structures of the Ti−POM peroxo and hydroperoxo complexes were also investigated by means of density-functional theory (DFT) calculations. The theoretical investigations carried out by few groups[51] have shown that presently the DFT calculations are accurate enough to reproduce the X-ray geometries of a POM[52] and the small energy differences between α and β isomers in Keggin[53] and Wells−Dawson[54] anions or even to determine the magnetic coupling between localized and delocalized electrons.[55]

Experimental Section

Materials and POMs. Acetonitrile (Fluka, HPLC quality) was dried and stored over activated 3 Å molecular sieves. TMP was purchased from Fluka and recrystallized from hexane. Tetra-*n*-

(17) Tozzola, G.; Mantegazza, M. A.; Ranghino, G.; Petrini, G.; Bordiga, S.; Ricchiardi, G.; Lamberti, C.; Zulian, R.; Zecchina, A. *J. Catal.* **1998**, *179*, 64−71.
(18) Bordiga, S.; Damin, A.; Bonino, F.; Ricchiardi, G.; Lamberti, C.; Zecchina, A. *Angew. Chem., Int. Ed.* **2002**, *41*, 4734−4737.
(19) Munukata, H.; Oumi, Y.; Miyamoto, A. *J. Phys. Chem. B* **2001**, *105*, 3493−3501.
(20) Crocker, M.; Herold, R. H. M.; Orpen, A. G.; Overgaag, T. A. *J. Chem. Soc., Dalton Trans.* **1999**, 3791−3804.
(21) Lorenz, V.; Fischer, A.; Giessmann, S.; Gilje, J. W.; Gun'ko, Y.; Jacob, K.; Edelmann, F. T. *Coord. Chem. Rev.* **2000**, *206−207*, 321−368.
(22) Pescarmona, P. P.; Van der Waal, J. C.; Maxwell, I. E.; Maschmeyer, T. *Angew. Chem., Int. Ed.* **2001**, *40*, 740−743.
(23) Fujiwara, M.; Wessel, H.; Hyung-Suh, P.; Roesky, H. W. *Tetrahedron* **2002**, *58*, 239−243.
(24) Thomas, J. M.; Sankar, G.; Klunduk, M. C.; Attfield, M. P.; Maschmeyer, T.; Johnson, B. F. G.; Bell, R. G. *J. Phys. Chem. B* **1999**, *103*, 8809−8813.
(25) Pope, M. T. *Heteropoly and Isopoly Oxometalates*; Springer: Berlin, 1983.
(26) *Polyoxometalates: From Platonic Solids to Anti-Retroviral Activity*; Pope, M. T., Müller, A., Eds.; Kluwer: Dordrecht, The Netherlands, 1993.
(27) *Polyoxometalate Chemistry From Topology via Self-Assembly to Applications*; Pope, M. T., Müller, A., Eds.; Kluwer: Dordrecht, The Netherlands, 2001.
(28) Hill, C. L.; Prosser-McCartha, C. M. *Coord. Chem. Rev.* **1995**, *143*, 407−455.
(29) Neumann, R. *Prog. Inorg. Chem.* **1998**, *47*, 317−370.
(30) Finke, R. G.; Rapko, B.; Saxton, R. J.; Domaille, P. J. *J. Am. Chem. Soc.* **1986**, *108*, 2947−2960.
(31) Chen, Q.; Zubieta, J. *Coord. Chem. Rev.* **1992**, *114*, 107−167.
(32) Baker, L. C. W.; Glick, D. C. *Chem. Rev.* **1998**, *98*, 3−49.
(33) Pope, M. T.; Müller, A. *Angew. Chem., Int. Ed. Engl.* **1991**, *30*, 34−48.
(34) Ma, L.; Liu, S.; Zubieta, J. *Inorg. Chem.* **1989**, *28*, 175−177.
(35) Mohs, T. R.; Du, Y. H.; Plashko, B.; Maatta, E. A. *Chem. Commun.* **1997**, 1707−1708.
(36) Kholdeeva, O. A.; Maksimov, G. M.; Maksimovskaya, R. I.; Kovaleva, L. A.; Fedotov, M. A.; Grigoriev, V. A.; Hill, C. L. *Inorg. Chem.* **2000**, *39*, 3828−3837.
(37) Kholdeeva, O. A.; Kovaleva, L. A.; Maksimovskaya, R. I.; Maksimov, G. M. *J. Mol. Catal., A: Chem.* **2000**, *158*, 223−229.
(38) Kholdeeva, O. A.; Maksimovskaya, R. I.; Maksimov, G. M.; Kovaleva, L. A. *Kinet. Catal.* **2001**, *42*, 217−222.
(39) Maksimov, G. M.; Kuznetsova, L. I.; Matveev, K. I.; Maksimovskaya, R. I. *Koord. Khim.* **1985**, *11*, 1353−1357 (in Russian).
(40) Yamase, T.; Ozeki, T.; Motomura, S. *Bull. Chem. Soc. Jpn.* **1992**, *65*, 1453−1459.
(41) Mimoun, H.; Postel, M.; Casabianca, F.; Fisher, J.; Mitschler, A. *Inorg. Chem.* **1982**, *21*, 1303−1306.
(42) Ledon, H. J.; Varescon, F. *Inorg. Chem.* **1984**, *23*, 2735−2737.
(43) Yamase, T.; Ishikawa, E.; Asai, Y.; Kanai, S. *J. Mol. Catal., A: Chem.* **1996**, *114*, 237−245.
(44) Postel, M.; Casabianca, F.; Gauffreteau, Y. *Inorg. Chim. Acta* **1986**, 173−180.
(45) Sisemore, M. F.; Selke, M.; Burstyn, J. N.; Valentine, J. S. *Inorg. Chem.* **1997**, *36*, 979−984.
(46) Kholdeeva, O. A.; Maksimov, G. M.; Maksimovskaya, R. I.; Kovaleva, L. A.; Fedotov, M. A. *React. Kinet. Catal. Lett.* **1999**, *66*, 311−318.
(47) Yudanov, I. V.; Gisdakis, P.; Di Valentin, C.; Rosch, N. *Eur. J. Inorg. Chem.* **1999**, *12*, 2135−2145.
(48) Zhidomirov, G. M.; Yakovlev, A. L.; Milov, M. A.; Kachurovskaya, N. A.; Yudanov, I. V. *Catal. Today* **1999**, *51*, 397−410.
(49) Trukhan, N. N.; Romannikov, V. N.; Paukshtis, E. A.; Shmakov, A. N.; Kholdeeva, O. A. *J. Catal.* **2001**, *202*, 110−117.
(50) Kholdeeva, O. A.; Trukhan, N. N.; Vanina, M. P.; Romannikov, V. N.; Parmon, V. N.; Mrowiec-Białoń, J.; Jarzębski, A. B. *Catal. Today* **2002**, *75*, 203−209.
(51) (a) Poblet, J. M.; López, X.; Bo, C. *Chem. Soc. Rev.* **2003**, in press. (b) Rohmer, M.-M.; Bénard, M.; Blaudeau, J.-P.; Maestre, J. M.; Poblet, J. M. *Coord. Chem. Rev.* **1998**, *178−180*, 1019−1049.
(52) (a) Bridgeman, A.; Cavigliasso, G. *J. Phys. Chem. A* **2002**, *106*, 6114−6120. (b) Bridgeman, A.; Cavigliasso, G. *Inorg. Chem.* **2002**, *41*, 1761−1770.
(53) López, X.; Maestre, J. M.; Bo, C.; Poblet, J. M. *J. Am. Chem. Soc.* **2001**, *123*, 9571−9576.
(54) López, X.; Bo, C.; Poblet, J. M.; Sarasa, J. P. *Inorg. Chem.* **2003**, *42*, 2634−2638.
(55) Duclusaud, H.; Borshch, S. A. *J. Am. Chem. Soc.* **2001**, *123*, 2825−2829.

butylammonium hydroxide ((TBA)OH) (1.0 M solution in MeOH, Aldrich) was titrated with HCl (0.1 M) prior to use. Hydrogen peroxide (35%) was titrated iodometrically. D_2O_2 was obtained by dilution of concentrated H_2O_2 (95%) in D_2O. All the other compounds were the best available reagent grade and were used without further purification. Peroxo complex **2** was prepared from the α-Keggin monomer $[TBA]_5[PTiW_{11}O_{40}]$ and H_2O_2 as described earlier[36] (^{31}P NMR: δ −13.0 ppm in MeCN). The μ-oxo dimer $[Bu_4N]_8[(PTiW_{11}O_{39})_2O]$ (**3**) was obtained from the μ-hydroxo dimer $[Bu_4N]_7[(PTiW_{11}O_{39})_2OH]$ (**4**)[36] by adding 1 equiv of methanolic (TBA)OH to a MeCN solution of **4** followed by precipitation of **3** with an excess of ether (IR (1200−400, cm^{-1}) ν 1065, 960, 880, 800, 640, 585, 520, 500; ^{31}P NMR (0.02 M in dry MeCN, 20 °C) singlet at δ −13.29; ^{183}W NMR (0.05 M in MeCN, 20 °C) −δ 92.1(2), 94.6(2), 95.2(1), 100.1(2), 112.2(2), 113.0(2)).

Synthesis and Characterization of $[Bu_4N]_4[HPTi(O_2)W_{11}O_{39}]$ (1). A 1.43 g (0.4 mmol) of **3** was dissolved in 10 mL of MeCN, and then 510 μL of 35% aqueous H_2O_2 (6.0 mmol) was added under stirring, yielding an orange solution of **1**. Unstable orange crystals of **1** were grown upon slow concentration of the solvent at room temperature. The crystals were filtered off, washed with MeCN, dried, and kept in a freezer compartment. Yield: 0.858 g (60.0%). The number of TBA cations, determined by ignition of **1** at 600 °C, was ca. 4.0/1 P atom. Iodometric titration revealed the presence of one peroxo group/molecule of **1**. Anal. Calcd for $C_{64}H_{145}N_4O_{41}PTiW_{11}$ (M_r = 3727.9): C, 20.62; H, 3.92; N, 1.50; P, 0.83; Ti, 1.28; W, 54.25. Found: C, 20.10; H, 3.83; N, 1.47; P, 0.79; Ti, 1.25; W, 54.70. ^{31}P NMR [δ (ppm); 0.02 M in dry MeCN at 20 °C]: −12.35 ($\Delta\nu_{1/2}$ = 3 Hz). ^{183}W NMR [δ (ppm); 0.05 M in MeCN at 20 °C]: −89.5, −98.5, −99.2, −101.5, −105.4, −108.7 with the approximate intensity ratio 2:2:1:2:2:2, respectively. Potentiometric titration of **1** (0.05 mmol) in MeCN (5 mL) with methanolic (TBA)OH showed a sharp breakpoint at 1 equiv of OH^- indicating a $[H^+]/[\mathbf{1}]$ ratio of 1.0. $[Bu_4N]_4[DPTi(O_2)W_{11}O_{39}]$ was obtained by using D_2O_2 instead of H_2O_2 as described in the literature.[56,57] X-ray-quality orange crystals of **1** (thin plates with dimensions 0.19 × 0.13 × 0.03 mm^3, tetragonal crystal system, space group $I\bar{4}$) were grown upon slow evaporation of $MeCN/H_2O_2/H_2O$ solution. However, the anion was statistically disordered due to the highly symmetric space group and the position of the TiOO species was therefore impossible to determine using X-ray single-crystal structure analysis.

Interaction of 1 with TMP. Stoichiometric reaction between TMP and **1** was performed under Ar in thermostated glass vessels equipped with a magnetic stirrer at [**1**] = 0.02 M and [TMP] = 0.01−0.04 M in dry MeCN (1 mL) at 40 °C. The catalytic TMP oxidation by H_2O_2 in the presence of **1** was carried out at [TMP] = 0.1, $[H_2O_2]$ = 0.35, and [**1**] = 0.01 M in MeCN (1 mL) at 40 and 80 °C. The reaction course was monitored using both ^{31}P NMR and GC. The oxidation products were identified by GC-MS and ^{1}H NMR and quantified by GC using biphenyl as internal standard.

Instrumentation and Methods. GC analyses were performed using a "Tsvet-500" gas chromatograph equipped with a flame ionization detector and a quartz capillary column (25 m × 0.3 mm) filled with Carbowax 20 M (Ar, 110−230 °C, 10°/min). GC-MS analyses of organic products were conducted using a Saturn 2000 gas chromatograph equipped with a CP-3800 mass spectrometer. ^{1}H NMR spectra were recorded on a DPX-250 Bruker spectrometer. ^{31}P and ^{183}W NMR spectra were recorded at 161.98 and 16.67 MHz, respectively, on an MSL-400 Bruker spectrometer. Chemical shifts, δ, were referenced to 85% H_3PO_4 and 1 M aqueous Na_2WO_4 for ^{31}P and ^{183}W NMR spectra, respectively. Chemical shifts upfield from the reference were reported as negative. In ^{31}P NMR measurements, a secondary standard, 0.1 M aqueous $H_4PVMo_{11}O_{40}$, was used. Its chemical shift, δ, −3.70 ± 0.03 ppm relative to concentrated H_3PO_4, was corrected for the solution magnetic susceptibility difference. The error in measuring δ was in the range ±0.04 and ±0.1 ppm for ^{31}P and ^{183}W NMR spectra, respectively. Infrared spectra were recorded as 0.5−2.0 wt % samples in KBr pellets or in MeCN solutions using KBr cells on a Specord 75 IR or a Shimadzu FTIR-8300 spectrometer. Electronic absorption spectra were run on a Shimadzu UV−vis 2501PC spectrophotometer using a 1-cm thermostated quartz cells. Raman spectra were recorded with a Triplemate, SPEX spectrometer with a LN-1340PB CCD detector from Princeton Instruments. The 514.5 and 488 nm lines of an Ar laser and 632.3 nm line of a He−Ne laser were used for spectral excitation. The spectra were obtained in backscattering geometry. The laser beam was focused to a diameter of 2 μm using a LD-EPIPLAN, 40/0.60 Pol., Zeiss objective. The spectral resolution was 2 cm^{-1}. The spectra were collected for about 1−2 min. The laser output power was about 30 mW, and the power on the sample surface was about 1 mW. Raman spectra in near-IR region (excitation at 1064 nm) were taken with a Fourier Raman spectrometer RFS-100/S. All the cyclic voltammetric measurements were performed at 25 °C under argon using a three-electrode cell, a glassy-carbon working electrode, a platinum auxiliary electrode, and a Ag/AgCl reference electrode. $(TBA)ClO_4$ (0.1 M in MeCN) was used as supporting electrolyte. The elemental analysis was done at Kanti Labs (Mississauga, Ontario, Canada).

Computational Details. All the calculations presented here were carried out using the density-functional methodology, implemented in the ADF2001 program.[58] We used the local density approximation (LDA) characterized by the electron gas exchange (Xα) with α = 2/3, together with the Vosko−Wilk−Nusair[59] (VWN) parametrization for correlation. Becke[60] and Perdew[61] gradient corrections were used for the exchange and correlation energy, respectively. The basis functions were Slater-type sets. Triple-ζ + polarization basis sets were used to describe the valence electrons of all the atoms. The internal or core electrons (1s and 2s shells for phosphorus, 1s to 2sp for titanium, and 1s to 4spd for tungsten) were described by means of single Slater functions. Quasirelativistic corrections were used for the core electrons alongside the Pauli formalism with corrected core potentials. The quasirelativistic frozen core shells were generated with the auxiliary program DIRAC,[58] included in the ADF2001 package. The discussion of all the anions is based on the fully optimized geometries, and the solvent effects were included by means of the conductor-like screening model (COSMO) software using the optimized geometries for the isolated anions.[62]

(56) Ho, R. Y. N.; Roelfes, G.; Feringa, B. L.; Que, L. *J. Am. Chem. Soc.* **1999**, *121*, 264−265.
(57) Simaan, A. J.; Dopner, S.; Banse, F.; Bourcier, S.; Bouchoux, G.; Boussac, A.; Hilderbrandt, P.; Girerd, J.-J. *Eur. J. Inorg. Chem.* **2000**, 1627−1633.
(58) *ADF 2000.01*; Department of Theoretical Chemistry, Vrije Universiteit: Amsterdam, 2000. Baerends, E. J.; Ellis, D. E.; Ros, P. *Chem. Phys.* **1973**, *2*, 41−51. Versluis, L.; Ziegler, T. *J. Chem. Phys.* **1988**, *88*, 322−328. Te Velde, G.; Baerends, E. J. *J. Comput. Phys.* **1992**, *99*, 84−98. Fonseca Guerra, C.; Snijders, J. G.; Te Velde, G.; Baerends, E. J. *Theor. Chem. Acc.* **1998**, *99*, 391−403.
(59) Vosko, S. H.; Wilk, L.; Nusair, M. *Can. J. Phys.* **1980**, *58*, 1200−1211.
(60) (a) Becke, A. D. *J. Chem. Phys.* **1986**, *84*, 4524−4529. (b) Becke, A. D. *Phys. Rev.* **1988**, *A38*, 3098−3100.
(61) (a) Perdew, J. P. *Phys. Rev.* **1986**, *B33*, 8882−8824. (b) Perdew, J. P. *Phys. Rev.* **1986**, *B34*, 7406.
(62) Pye, C. C.; Ziegler, T. *Theor. Chem. Acc.* **1999**, *101*, 396−403.

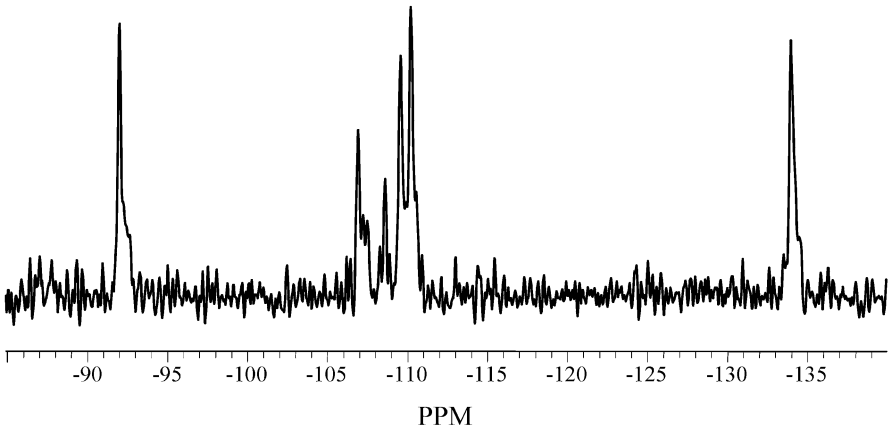

Figure 1. ^{183}W NMR spectrum of **1** in the presence of a 15-fold excess of 30% H_2O_2 (0.04 M in MeCN at 20 °C).

Results and Discussion

Synthesis and Characterization of $[Bu_4N]_4[HPTi(O_2)W_{11}O_{39}]$ (1). In our previous work, we obtained a protonated Ti−POM peroxo species (^{31}P NMR: δ −12.4) in situ by adding 1 equiv of H^+ (in the form of triflic acid) to **2** (δ −13.0 ppm).[36,37] Our attempts, however, to precipitate this species from the solution using a standard procedure by adding an excess of ether were unsuccessful because of its decomposition during the precipitation. Then we found by using ^{31}P NMR that interaction of the μ-oxo dimeric heteropolytungstate $[Bu_4N]_8[(PTiW_{11}O_{39})_2O]$ (**3**) with a 15-fold excess of 35% aqueous H_2O_2 in MeCN results in the formation of the protonated Ti−POM peroxo species, which can be described by eq 1.

$$[Bu_4N]_8[(PW_{11}O_{39}Ti)_2O] + 2H_2O_2 \rightleftarrows 2[Bu_4N]_4[HPTi(O_2)W_{11}O_{39}] + H_2O \quad (1)$$

Equation 1 predicts that the addition of H_2O would shift the equilibrium left. Both ^{31}P NMR and UV−vis confirm that this is precisely what happens. Slow concentration of the solution leads to orange crystals of **1**. By sharp contrast to unprotonated peroxo complex **2**, protonated species **1** is unstable and should be kept in a freezer. The purity of **1** was confirmed by using elemental analysis data, IR, cyclic voltammetry, and ^{31}P NMR spectroscopy.

The only peak detected in the ^{31}P NMR spectrum was a singlet at −12.35 ppm in MeCN (see Supporting Information (SI)). This chemical shift is very close to that observed for the protonated Ti−POM peroxo species generated in situ upon addition of 1 equiv of H^+ to **2**.[36] Potentiometric titration with methanolic (TBA)OH confirmed the presence of one acid proton in the molecule of **1** (see SI). The addition of 1 equiv of OH^- resulted in the formation of **2** (δ −13.0 ppm). Iodometric titration indicated the presence of one peroxo group/molecule of **1**.

The ^{183}W NMR spectrum of **1** run under conditions of an excess of H_2O_2 to prevent its decomposition during the acquisition time consists of six lines with an intensity ratio of 2:2:1:2:2:2 (Figure 1), indicating a C_s symmetry for the anion or a fast proton exchange on the NMR time scale. Unfortunately, the solubility of **1** in MeCN was low, so the signal-to-noise ratio in the ^{183}W NMR spectrum was rather poor. Note that both ^{31}P and ^{183}W NMR spectra of **1** differ significantly from the same spectra of **2**.[39,40]

An attempt was made to perform a single-crystal X-ray analysis of **1**. The monomeric Keggin structure of **1** has been confirmed, which is important because dimeric (μ-peroxy)-titanium complexes are precedented.[63,64] Unfortunately, the anion was statistically disordered due to the highly symmetric space group ($I\bar{4}$), and the position of the TiOO species was impossible to determine. Earlier, Yamase's group faced the same problem when they studied $[(i\text{-}C_3H_7)_2NH_2]_5[PTi(O_2)W_{11}O_{39}]\cdot 4H_2O$ by using X-ray.[40] Note that crystal disordering is a typical phenomenon for $[XM'M_{11}O_{39}]^{n-}$ heteropolyanions.[25]

Contrary to the NMR spectra, which are very sensitive to protonation,[30,36] both electronic and vibrational spectra of **1** and **2** are very similar, indicating the similarity of their structures. The UV−vis spectra of **1** and **2** show a strong absorption with maxima at 395 (see SI) and 390 nm, respectively, which is attributed to the $O_2 \rightarrow$ Ti ligand-to-metal charge-transfer band.[39,40] The resonance Raman (RR) spectra of **1** and **2** taken with excitation at $\lambda = 488$ or 514 nm display an intense band at 630 cm^{-1} (Figure 2). This band is not observed in the Raman spectra of the original, colorless Ti−POMs and according to literature can be assigned to the symmetric Ti−O_2 stretching vibration of the peroxide group.[18,65,66] This assignment is confirmed by a strong resonance behavior of the band, the intensity of which gradually decreases with increasing excitation λ (Figure 3) or upon slow decomposition of **1**. Noteworthy, a strong band at 618 cm^{-1} has been observed in RR spectrum of TS-1 after treatment with H_2O_2/H_2O.[18]

Characteristic features of the IR spectra of **1** and **2** are two bands observed at 630 and 690 cm^{-1} and 620 and 714 cm^{-1}, respectively (Figure 4). The absence of these bands in the IR spectra of the peroxo free Ti−POMs[36] suggests that they can be attributed to the symmetric and asymmetric

(63) Schwarzenbach, G. *Inorg. Chem.* **1970**, *9*, 2391−2397.
(64) Muhlebach, J.; Muller, K.; Schwarzenbach, G. *Inorg. Chem.* **1970**, *9*, 2381−2390.
(65) Griffith, W. P.; Wickins, T. D. *J. Chem. Soc. A* **1968**, 397−400.
(66) Kakihana, M.; Tada, M.; Shiro, M.; Petrykin, V.; Osada, M.; Nakamura, Y. *Inorg. Chem.* **2001**, *40*, 891−894.

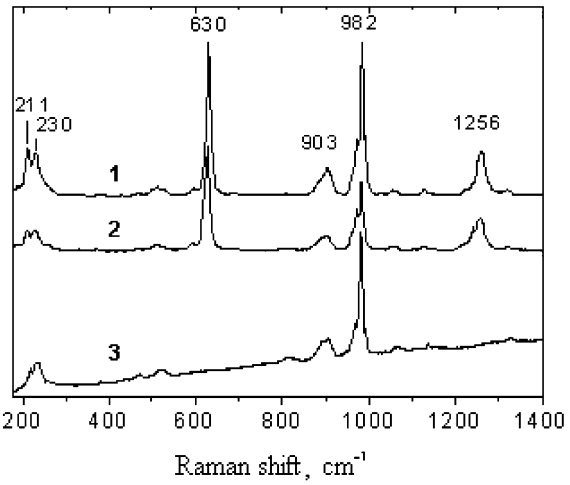

Figure 2. Resonance Raman spectra of solid **1**, **2**, and $[TBA]_5[PTiW_{11}O_{40}]$ (curve 3) (λ_{exc} = 488 nm).

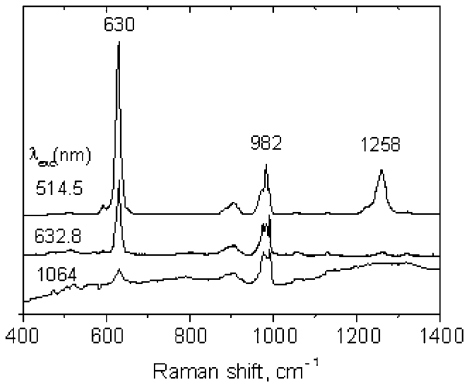

Figure 3. Resonance Raman spectra of solid **1** taken at different excitation λ values.

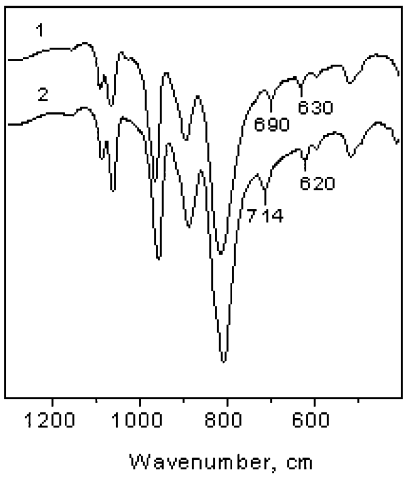

Figure 4. FTIR spectra of **1** and **2**. Both samples are 0.5 wt % in KBr.

metal−peroxide stretches.[41,65,67] Thus, both IR and RR provide evidence in favor of the side-on (η_2) bonding mode of the peroxo ligand. Note, the η^2-structure for (hydroperoxo)titanium species was supported by density functional calculations carried out on titanium−silicates.[68−70] Importantly, the IR and RR spectra of **1** are very close in both solid state and MeCN solution, which confirms the retention of the η_2-structure in solution. The O−O stretching band, which is known to manifest around 900 cm^{-1} for mono-peroxo complexes,[41,65,67,71,72] is not seen in the IR spectra of **1** and **2** due to overlap with the strong W−O−W asymmetric stretch (895 cm^{-1}) of the Keggin unit (Figure 4).

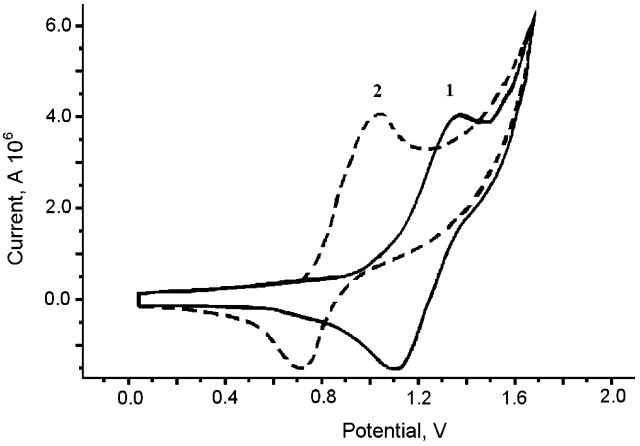

Figure 5. Cyclic voltammetric curves for **1** and **2** (0.005 M in MeCN). Potentials are reported relative to a standard Ag/AgCl electrode. Scan rate: 100 mV/s. Supporting electrolyte: 0.1 M $(TBA)ClO_4$.

Cyclic voltammetry performed at +1.7−0 V showed a peak at $E_{1/2}$ = 1.25 V relative to Ag/AgCl reference electrode (Figure 5). No CV peaks were detected in the above potential range for the peroxo-free Ti−POMs.[36] According to literature,[73] this wave can be assigned to reduction/oxidation of the peroxo group. Peroxo complex **2** displays a similar redox behavior but shows a lower redox potential ($E_{1/2}$ = 0.88 V). Thus, we may conclude that the protonation results in an increase of the oxidizing ability of the peroxytitanium group.

Stoichiometric Oxidation of TMP by 1. Like other known titanium peroxo complexes,[41,42,44,45] unprotonated species **2** was found to be inert toward organic substrates.[36,43] In our previous study, we demonstrated that the protonated Ti−POM peroxo complex, generated in situ from **2** and H^+, interacts with organic sulfides under both stoichiometric and turnover conditions.[36−38] An outer-sphere electron-transfer mechanism involving the formation of a radical cation has been proposed based on the product and kinetic studies.[37] In this work, we found that **1**, by sharp contrast to **2**, readily reacts with TMP at 40 °C in MeCN to give TMBQ and the corresponding C−C-coupling product, 2,2′,3,3′,5,5′-hexamethyl-4,4′-biphenol (BP) (eq 2).

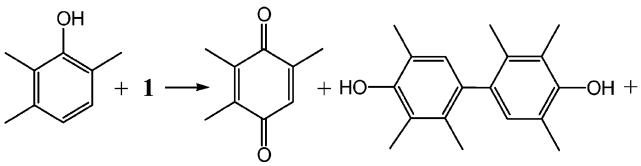

$$[Bu_4N]_4[PTi(OH)W_{11}O_{39}] + H_2O \quad (2)$$

Disappearance of the ^{31}P NMR signal of **1** at δ −12.35 ppm along with simultaneous appearance of the Ti−POM

(67) Butler, A.; Clague, M. J.; Meister, G. E. *Chem. Rev.* **1994**, *94*, 625−638.
(68) Wu, Y.-D.; Lai, D. K. W. *J. Am. Chem. Soc.* **1995**, *117*, 11327−11336.
(69) Barker, C. M.; Gleeson, D.; Kaltsoyannis, N.; Catlow, C. R. A.; Sankar, G.; Thomas, J. M. *Phys. Chem. Chem. Phys.* **2002**, *4*, 1228−1240.

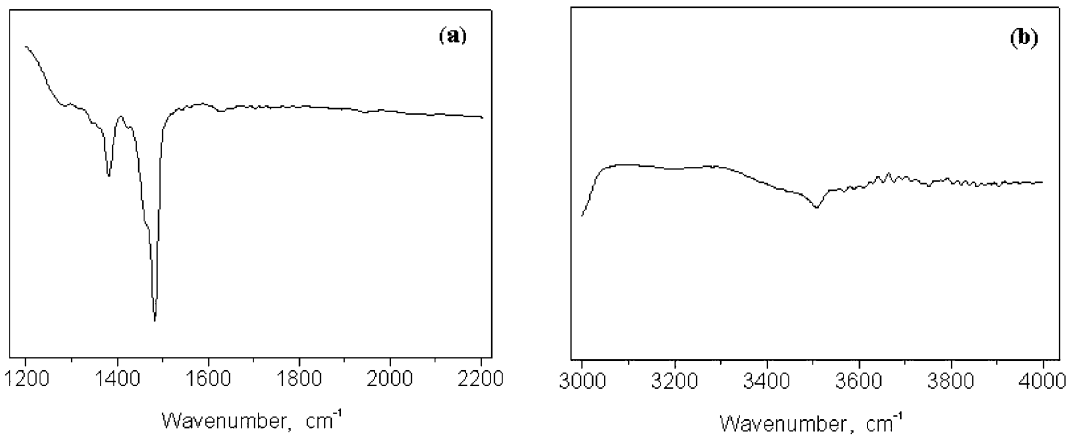

Figure 6. IR spectrum of **1** (0.5 wt % in KBr) in the range of (a) 1200−2100 cm^{-1} and (b) 3000−4000 cm^{-1}.

peaks at −13.34 and −13.27 ppm, which most likely belong to $[Bu_4N]_4[PTi(OH)W_{11}O_{39}]$[36] and $[Bu_4N]_4[PTi(OAr)W_{11}O_{39}]$, respectively, was observed. The intensity of the signal at δ −13.27 ppm enhanced with increasing initial TMP concentration. The disappearance of **1** was also detected using UV−vis. Significantly, in the absence of TMP the rate of the decay of **1** was 1 order of magnitude lower. The ratio between the TMP oxidation products dramatically depends on [TMP]/[**1**]. When a 2-fold excess of TMP was used, the main reaction product was BP (90%), while a 2-fold excess of **1** led to TMBQ (95%). This agrees with the reaction stoichiometry 2:1 and 1:2 for the TMP oxidation to BP and TMBQ, respectively. The TMP oxidation occurs smoothly under turnover conditions ($[H_2O_2]/[\mathbf{1}] = 35$). At [TMP] = 0.1, $[H_2O_2] = 0.35$, and [**1**] = 0.01 M, complete TMP conversion to BP and TMBQ (BP/TMBQ = 3.0) was achieved after 2 h at 80 °C. At 40 °C, TMP conversion was 45% after 2 h, while the BP/TMBQ ratio was the same. The formation of BP, a typical one-electron oxidation product, allows us to suggest a homolytic oxidation mechanism that implicates the formation of phenoxyl radicals ArO•.[74] The radical coupling gives BP, while further interaction with **1** leads to TMBQ. Interestingly, the same products and analogous effect of the TMP/Ti ratio on the product distribution were found in the TMP oxidation with H_2O_2 catalyzed by mesoporous Ti−MMM catalysts.[49,50] Earlier, we also observed similarities in the catalytic behavior of Ti−POMs and Ti−MMM in thioether oxidation with H_2O_2.[38] It is well-known that the mechanism of oxidation with H_2O_2 in the presence of Ti,Si catalysts depends on both the nature of the organic substrate and the catalyst. Both homolytic and heterolytic reaction pathways may operate.[3] Keeping in mind our previous results on the thioether oxidation[36−38] and the results obtained in this work, we may propose **1** as a model compound for studying homolytic mechanisms of titanium-catalyzed oxidations. Again, the presence of a proton in the molecule of **1** is crucial for its reactivity. One of the possible explanations of this phenomenon is the increase of the redox potential of the peroxo group upon protonation (vide infra); however, the proton may also facilitate the formation of a reactive η^1-intermediate in solution.[3,42] DFT calculations carried out on the Ti−POM peroxo derivatives (vide supra) support the latter hypothesis. Significantly, **1** is not reactive toward alkene epoxidation. Meanwhile, our preliminary data showed that further protonation of **1** leads to the formation of highly protonated Ti−POM peroxo species, which are capable of oxygen transfer reactions, and a forthcoming paper will be devoted to this matter.

Localization of the Activating Proton in 1. Finally, we address the question about the site of the activating proton in **1**. No IR bands were observed for solid **1** in the 1800−1600 cm^{-1} region (Figure 6a) indicating that no H_3O^+ was present and that the proton is directly attached to the POM surface.[30] The W═O and W−O−W oxygen atoms are less likely as possible sites for protonation since metals with higher charge are more electron withdrawing, thereby decreasing the nucleophilicity of the oxygen atom at a given pH.[75] Thus, both a peroxo oxygen atom and a Ti−O−W bridging oxygen were regarded as possible protonation sites.[36] However, if the proton were attached to the peroxo group, a characteristic H/D downshift of the RR band would be expected, as observed for iron hydroperoxo species.[56,57] We prepared **1** using D_2O_2 instead of H_2O_2 and found that the 630 cm^{-1} feature in the RR is not sensitive to the replacement of H for D. Therefore, the activating proton is most likely located at the Ti−O−W bridge rather than at the peroxo group. The bridging OH manifests in the IR spectrum of solid **1** at 3510 cm^{-1} (Figure 6b). Both the frequency and width ($\Delta\eta = 30$ cm^{-1}) of the OH stretching band indicate the presence of hydrogen bonding.[76]

DFT Calculations. Conclusions concerning the structure of **1** based on the experimental findings are in agreement

(70) Tantanak, D.; Vincent, M. A.; Hillier, I. H. *J. Chem. Soc., Chem. Commun.* **1998**, 1031−1032.
(71) (a) Latour, J.-M.; Galland, B.; Marchon, J.-C. *J. Chem. Soc., Chem. Commun.* **1979**, 570−571. (b) Reynolds, M. S.; Butler, A. *Inorg. Chem.* **1996**, *35*, 2378−2383.
(72) Qu, L.-Y.; Shan, Q.-J.; Gong, J.; Lu, R.-Q.; Wang, D.-R. *J. Chem. Soc., Dalton Trans.* **1997**, 4525−4528.
(73) Meng, L.; Zhan, X. *Transition Met. Chem.* **2001**, *26*, 448−450.
(74) Taylor, W. I. *Oxidative Coupling of Phenols*; Marcel Dekker: New York, 1967.
(75) Kepert, D. L. *The Early Transition Metals*; Academic Press: London, 1972; p 47.
(76) Jeffrey, G. A. *An introduction to hydrogen bonding*; Oxford University Press: New York, 1997; p 303.

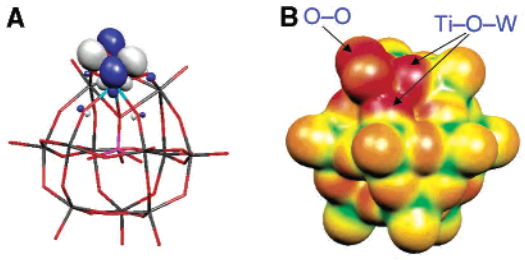

Figure 7. (A) Representation of the HOMO for the eclipsed peroxo form. (B) Molecular electrostatic potential function plotted over an isodensity surface for the same structure. Red regions represent proton-attractive sites.

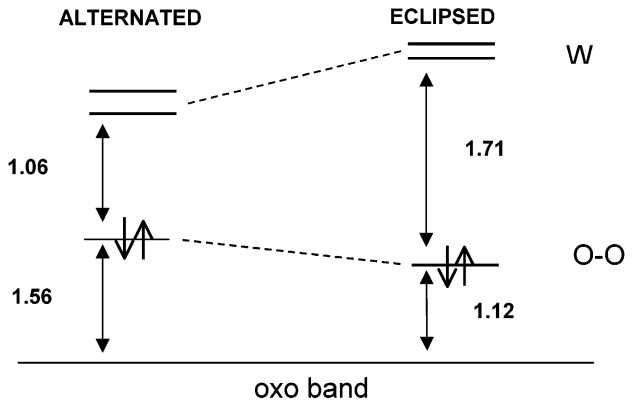

Figure 8. Schematic representation of the frontier orbitals of an alternated peroxo structure and the theoretically most stable eclipsed form. The energy gaps (in eV) vary as a consequence of the geometry change.

Chart 1

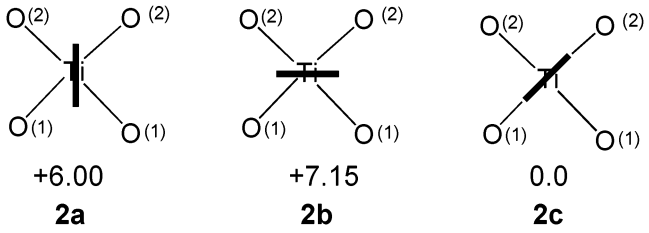

with DFT calculations performed for $[PTi(O_2)W_{11}O_{39}]^{5-}$ and its protonated partner. To obtain the geometry of minimal energy for the nonprotonated complex, three orientations of the peroxo group were explored for the $[PTi(O_2)W_{11}O_{39}]^{5-}$ anion. Two orientations were computed under the restrictions of the C_s point group, labeled **2a**,**b** in Chart 1 (their relative energies are indicated in kcal mol^{-1}), one of them with the σ-plane containing the Ti center and the O_2 group (**2a**) and the other one with the peroxo group perpendicular to σ (**2b**).

Both conformations are very similar in energy, only differing by a mere 1.15 kcal mol^{-1}. The third structure, **2c**, of C_1 symmetry, in which the peroxo group is almost aligned with the O−Ti−O plane, is clearly more stable (6−7 kcal mol^{-1}) than the conformations where the O_2 ligand is rotated ∼45° with respect to the eclipsed conformation. This latter orientation permits electron donation from the occupied π^*_{O-O} orbital to the vacant d_{xy}(Ti)-like orbital by in-phase π^*−d overlapping (Figure 7A). Such an effect produces an extra stabilization of the HOMO of **2c**, being 0.3−0.4 eV lower in energy than in the *alternated* homologues (Figure 8). The bond lengths computed for O−O and O−Ti in the most stable eclipsed conformation are 1.50 and 1.90 Å, respectively. It is worth mentioning that POM geometries are very well reproduced by DFT methods, with average deviations from X-ray data of about 0.03 Å.[51,53,77] The only exception corresponds to the metal−terminal oxygen distances, which are, in general, overestimated by ∼0.05 Å. The O(1) oxygens link the TiW_2 triad with another triad (corner-sharing) whereas O(2) are bridging oxygens inside the TiW_2 triad (edge-sharing). According to the formal IV and VI oxidation states for Ti and W, respectively, the electronic structure of $[PTi(O_2)W_{11}O_{39}]^{5-}$ is characterized by two sets of orbitals relatively close in energy. The HOMO in the nonprotonated species is fairly localized over the O−O group, and the empty set of d-metal orbitals appear 1.71 eV above the occupied band at the DFT level, which is a somewhat small value compared to ∼2.90 eV of the related $[PTiW_{11}O_{40}]^{5-}$ Keggin anion. This could be a sign of higher reactivity of the peroxo derivative. Structures **2a**,**b** have smaller HOMO−LUMO gaps, very close to 1.0 eV.

In principle, the reaction of $[Bu_4N]_8[(PW_{11}O_{39}Ti)_2O]$ with H_2O_2 could yield a peroxo complex with the peroxo ligand coordinated to the Ti ion or to one of the 11 tungstens. For $[PW(O_2)TiW_{10}O_{39}]^{5-}$ there are six distinct isomers according to the position of $W(O_2)$ in relation to Ti. Since we do not expect a strong energy dependence of the cluster with the $W(O_2)$ position, we have arbitrarily chosen one nonneighboring $W(O_2)$−Ti form to determine the energy of $[PW(O_2)TiW_{10}O_{39}]^{5-}$ with respect to that of $[PTi(O_2)W_{11}O_{39}]^{5-}$. In the eclipsed conformation for the O_2 group, the $W(O_2)$ complex was computed to be 13.7 kcal mol^{-1} above the most stable conformation for $[PTi(O_2)W_{10}O_{39}]^{5-}$ (**2c**). This important energy excludes the $[PW(O_2)TiW_{10}O_{39}]^{5-}$ peroxo complex as a result of the reaction of $[Bu_4N]_8[(PW_{11}O_{39}Ti)_2O]$ with H_2O_2.

A priori, the protonation of $[PTiW_{11}O_{40}]^{5-}$ could yield several isomers depending on the protonation site and the orientation of the proton. The electrostatic potential (EP) function is a useful tool in the prediction of protonation sites in a POM, allowing a qualitative classification of the relative nucleophilicity of the external regions of the POM core.[77,78] Alternatively, the protonation sites can be studied by explicit addition of protons in an attempt to find quantitative relative protonation energies.[78,79] Previous calculations have shown that the basicity scale of the external oxygens in a POM is well classified by the DFT methodology.[51] In the present case, the search for the most basic site of $[PTi(O_2)W_{11}O_{39}]^{5-}$ was analyzed through the calculation of the structures represented in Figure 9. The EP function was found suitable for discriminating the most from the least favorable proto-

(77) (a) Maestre, J. M.; López, X.; Bo, C.; Casañ-Pastor, N.; Poblet, J. M. *J. Am. Chem. Soc.* **2001**, *123*, 3749−3758. (b) Bridgeman, A. J.; Cavigliasso, G. *Inorg. Chem.* **2002**, *41*, 1761−1770. (c) Bridgeman, A. J.; Cavigliasso, G. *Inorg. Chem.* **2002**, *41*, 3500−3507.
(78) López, X.; Bo, C.; Poblet, J. M. *J. Am. Chem. Soc.* **2002**, *124*, 12574−12582.
(79) (a) Bardin, B. B.; Bordawekar, S. V.; Neurock, M.; Davis, R. J. *J. Phys. Chem. B* **1998**, *102*, 10817−10825. (b) Ganapathy, S.; Fournier, M.; Paul, J. F.; Delevoye, L.; Guelton, M.; Amoureux, J. P. *J. Am. Chem. Soc.* **2002**, *124*, 7821−7828.

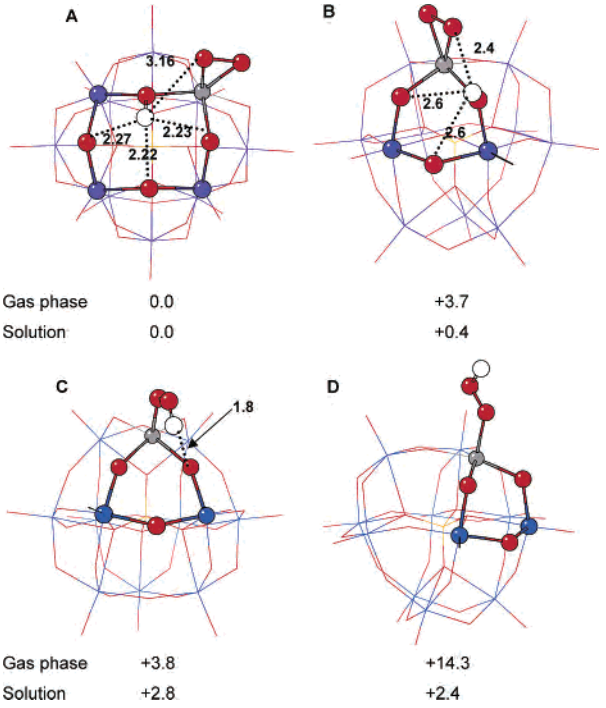

Figure 9. Optimized structures, relative energies (in kcal mol^{-1}), and H···O distances (in Å) for several isomers of $[HPTi(O_2)W_{11}O_{39}]^{4-}$. Notice the existence of a correlation between the number of H···O interactions and the stability.

nation sites in $[PTi(O2)W_{11}O_{39}]^{5-}$.[51b,80] The EP distribution was plotted over a 3D-density isosurface (Figure 7B). The red color identifies the most favorable protonation sites (nucleophilic regions). This representation suggests that the most likely positions to accept an incoming proton are the four oxygen atoms bridging the Ti and W atoms, indicated by the intense red color in those regions. Contrarily, terminal W═O sites would be the least basic ones and, in general, protonation in these terminal oxygens is very unlikely.[78] The O_2 group could compete in the protonation process because the EP takes similar values compared to Ti−O−W sites.

A more quantitative description was obtained through the study of the protonated species, $[HPTi(O_2)W_{11}O_{39}]^{4-}$. When the Ti−O−W oxygens were protonated, several local minima were found. In the most stable structure A (Figure 9A) the hydrogen is oriented toward the center of the nearest M_4O_4 ring, a region with a high proton affinity. Notice in Figure 7B the intense red area nearby the M_4O_4 ring, especially in the vicinity of the Ti−O−W sites. In structure B, the proton is roughly equidistant from two bridging oxygens and from one of the oxygens of the peroxo group. This form is 3.7 kcal mol^{-1} above the most stable structure A in the gas phase. The relative energies of these two proton orientations changes when the solvent is included via a continuum model.[62] In MeCN (dielectric constant = 37.0) the two conformations are only separated by 0.4 kcal mol^{-1}. In continuum-like models, the effects of a polar solvent upon the solute are purely electrostatic. The target molecule is surrounded by a surface that contains a set of point charges induced by the charge distribution of the molecule encapsulated. The distribution of point charges over the surface cavity is found so that it minimizes the energy of the solute. Both the energy of the solute and the distribution of point charges of the cavity are characterized by the dielectric constant of the solvent. The interaction between the surface point charges and the anion is more efficient in structure B because the proton is oriented outward from the anion surface and therefore more exposed to solvent effects.

Protonation of the peroxo ligand was also amply studied. All attempts to obtain a TiOO−H side-on coordination structure were, however, unsuccessful because the optimization always evolved toward geometries with a η^1-coordination. This result contrasts with the very recent B3LYP study of Sever and Root on the $Ti(OH)_3OOH$ model clusters, who also found structures with a η^2-coordination for the OOH group.[81] The conclusions of those authors cannot be directly applied to polyoxometalate chemistry because the titanium center always has an octahedral coordination and the basicity of Ti−O−W bonds is not well reproduced by a Ti−O−H bond. The relative energy of structure C (Figure 9) in relation to structure A is +3.8 kcal mol^{-1} in the gas phase and only +2.8 kcal mol^{-1} in MeCN solution. Structure D is quite unstable, presumably due to the lack of any stabilizing O···H interaction. But again, a large stabilization is observed when the effect of the solvent is included in the calculations. In this latter case, the proton is very exposed to the solvent molecules and the relative energy for D goes from +14.3 kcal mol^{-1} in the isolated anion to only +2.4 kcal mol^{-1} in solution. Therefore, although the calculations point to Ti−O−W as the most basic site, both Ti−OH−W and TiOO−H protonated anions could coexist in solution. Present calculations clearly show that, in addition to the intrinsic basicity of an oxygen site, inter- and intra-O···H interactions in POM clusters are of great importance in determining the protonation site in a POM.

It is worth noting that structure C (in which the O−O group has been protonated) yields the larger HOMO−LUMO gap of the series, a sign of stability of the cluster. The protonation at the peroxo ligand stabilizes the energy of the HOMO, which is only 0.1 eV above the oxo band. Contrarily, the protonation in the Keggin core, as expected, does not modify the relative energy of the frontier orbitals. Finally, let us comment that the Mulliken population analysis shows a small increment of the positive charge in all the metal centers after protonation, particularly in those centers closest to the proton, namely, the titanium atom and two of the four neighboring W atoms. The largest change amounts to 0.07 e.

Conclusions. The first protonated titanium peroxo complex **1** has been isolated and comprehensively characterized. A compilation of UV−vis, IR, RR, ^{31}P and ^{183}W NMR, cyclic voltammetry, potentiometric titration, and elemental analysis data supports a monomeric Keggin structure of **1** bearing one peroxo ligand in a η^2-coordination fashion. Deuterium labeling RR experiments revealed that the proton

(80) Maestre, J. M.; Sarasa, J. P.; Bo, C.; Poblet, J. M. *Inorg. Chem.* **1998**, *37*, 3071−3077.

(81) Sever, R. R.; Root, T. W. *J. Phys. Chem.* **2003**, *107*, 4080−4089.

is most likely localized at a Ti−O−W bridging oxygen rather than at the peroxo group. Protonated species **1** smoothly oxidizes TMP under both stoichiometric and turnover conditions to give the typical one-electron oxidation product, BP, along with TMBQ; the proportion between BP and TMBQ is affected by the TMP/**1** molar ratio. The obtained results allow us to suggest **1** as a soluble model compound for studying one-electron mechanisms of H_2O_2-based titanium-catalyzed oxidations. A detailed mechanistic study of its interaction with alkylphenols, including elucidation of the role of the activating proton, is in progress in our groups.

In agreement with the experimental characterization for **1** and **2**, the DFT calculations showed that the TiOO peroxo complex is much more stable than the WOO peroxo complex, the alternative product in the synthesis of **1**. Extensive calculations carried out on the protonated anion $[HPTi(O_2)W_{11}O_{39}]^{4-}$ suggest that the most stable hydroperoxo complex is formed preferentially after protonation of the Ti−O−W site that is the most intrinsic basic site. However, the TiOO−H form is strongly stabilized by interaction of the proton with the solvent and both Ti−OH−W and TiOO−H protonated anions could coexist in solution.

Acknowledgment. We thank Craig L. Hill for discussion and help. Financial support from the Russian Foundation for Basic Research (Grant 01-03-32852) is gratefully acknowledged. X.L. and J.M.P. thank the MCyT (Grant BQU2002-04110-C02-01) and the CIRIT (Grant SGR01-00315) for support.

Supporting Information Available: ^{31}P NMR, potentiometric titration, and UV−vis data for **1** and computed coordinates for several structures. This material is available free of charge via the Internet at http://pubs.acs.org.

IC0354466